

# TUNNEL DETECTION AND LOCALIZATION VIA MULTI-MONOSTATIC RF TOMOGRAPHY USING MAGNETIC SOURCES

**Francesco Soldovieri<sup>1</sup>, Lorenzo Lo Monte<sup>2</sup>, Danilo Erricolo<sup>3</sup>**

**1** Istituto per il Rilevamento Elettromagnetico dell'Ambiente" (IREA-CNR)

Consiglio Nazionale delle Ricerche, Napoli, Italy (e-mail: soldovieri.f@irea.cnr.it).

**2** General Dynamics Information Technology, Wright-Patterson Air Force Base,

Dayton, Ohio, 43441, USA, (e-mail: Lorenzo.lomonte.ctr@wpafb.af.mil).

**3** Department of Electrical and Computer Engineering, University of Illinois at Chicago,

Chicago, Illinois, 60607 USA (e-mail: erricolo@ece.uic.edu)

*An inverse scattering approach is presented to detect, localize and estimate the geometry of buried dielectric targets, in a 2D scenario, by exploiting magnetic sources as transmitting antennas. Explicit formulas to compute the scattered field from dielectric anomalies are derived for both homogeneous and half-space background scene. A linear inverse scattering approach is formulated and analysed for both the scenarios; finally, the performance of the two proposed approaches is tested against full-wave FDTD data simulating the exact scattering phenomenon.*

**Keywords: Ground Penetrating Radar, Microwave Tomography, Tunnel Detection**

## I. INTRODUCTION

This article investigates the detection, localization and geometry estimation (size and hopefully shape) of buried targets by enabling airborne ground penetrating radar (GPR) subsurface imaging. GPR has been extensively used to detect unexploded ordnance and landmines, as well as storage of weapons and adits. The novelty of this article is that it focuses on deeper penetration compared to usual airborne GPR, with the aim to image tunnels, underground facilities and deep targets, all of which interest civil and defence applications. To this end, systems radiating low frequency (of the order of MHz) electromagnetic fields have to be used and, in such cases, the operating wavelength is large compared to the dimension of the antenna. Since electrically small antennas have lower efficiency, electrically small loops loaded with ferrite coils [1] are used to improve efficiency and operating bandwidth. Electrically small loops are also relevant for subsurface imaging at low frequencies [2] as in the case of deep sounding in glacial inspection [3], Mars subsurface prospecting [4], and Radio Frequency Tomography to image buried dielectric/conducting anomalies such as tunnels, cavities and underground assets [5, 6, 7].

The search of underground objects using electromagnetic waves can be formulated as an inverse scattering problem [8, 9], where information about the buried targets is recovered from measurements of the scattered field collected by the receiving antennas. Specifically, this search is a subsurface imaging problem where the level of difficulty is simplest for the sole detection and localization of the target, then becomes more difficult to also estimate the object geometrical size, until it reaches the highest level of difficulty for the additional accurate determination of the electromagnetic nature/structure of the targets.

From a mathematical viewpoint, subsurface imaging is a special case of inverse scattering problem where, at microwave and radio-frequencies, targets are reconstructed in terms of a spatial map of their electromagnetic features, usually given in terms of dielectric permittivity [10, 11], electrical conductivity and, recently, magnetic permeability [12]. Inverse scattering problems are non-linear and ill-posed [8, 9] and their solution under an exact formulation generally requires to set up some optimization procedure (either deterministic or stochastic) [10, 13-15]. Non-linear imaging schemes still suffer from reliability problems due to the occurrence of false solutions (e.g. the functional to be minimized has local minima, which can trap the optimization procedure) [10, 13] and are computationally demanding in terms of both time and memory resources. Hence, they cannot be used to image electrically large spatial region when the time to compute an image is a constraint and the main aim is to obtain information about the location and geometry of the targets.

Moreover, for quantitative reconstructions, inverse scattering methods require the accurate knowledge of key elements at the basis of the scattering model, such as the incident field and the Green's functions pertinent to the scenario, which are in turn challenging inverse problems when realistic scenarios are tackled [16].

Nevertheless, the detection and localization of buried objects is the primary concern in many practical applications and can be successfully achieved by adopting imaging algorithms based on simplified scattering models, which neglect high-order effects due to mutual interactions and, accordingly, linearize the scattering equations [17-19]. In fact, the majority of subsurface imaging algorithms are implicitly or explicitly based on a linear assumption. This is because linear imaging algorithms for scatterers localization and shape estimation work well far beyond the limits of validity of the scattering linear models upon which they are based [20-22]. To summarize, a linear inverse problem has the following advantages:

- (i) Reliability because the problem does not have false solutions, contrary to non-linear inverse scattering problems;
- (ii) Existence of assessed regularization schemes able to counteract the effect of noise and uncertainties on data;
- (iii) Possibility to set up strategies to design non-redundant measurement configurations [23].
- (iv) Possibility to assess the reconstruction performance of the solution approach, which may be expressed in terms of retrievable spatial variability of the unknowns so to give a more thorough interpretation of the tomographic images .

Therefore, in this article we consider a linear imaging algorithm based on the Born approximation applied to subsurface imaging [17, 18, 24]. One novelty is the adoption of magnetic filamentary currents as sources (which can model accurately electrically small loops/coils) instead of the usual case of electric filamentary currents found in the literature. Another novel aspect regards the investigation of the performance of two linear inversion approaches, which differ for the choice of the background scenario. Initially, we consider a homogeneous background scenario, with the same properties of the underground, and later we improve it by considering a half-space with a planar interface.

The paper is organized as it follows. In Section II, the problem is given a general formulation by adopting a simplified model of the electromagnetic scattering. Section III is devoted at presenting the linear inverse problem by assuming a Green's function pertinent to a homogeneous medium, whereas in Section IV the Green's function relative to the actual half-space geometry is considered. Section V presents the Truncated Singular Value Decomposition scheme [25] used to invert the linear integral equation relating the unknown contrast function to the scattered field. Numerical results are

given in Section VI with the main aim of pointing out the performance of the linear inverse problem for the two formulations, according to the degree of regularization used in the inversion. Finally, Conclusions follow.

## II. FORMULATION OF THE PROBLEM

A two-dimensional reference half-space scenario is assumed, with the two media separated by a planar interface at  $z=0$ , as shown in Fig. 1. The upper medium (air) is free space, whereas the lower one (underground) has an equivalent complex dielectric permittivity  $\varepsilon_s$  to account also for losses; the magnetic permeability is everywhere the one of free-space  $\mu_s = \mu_0$ .

The source is an invariant  $z$ -directed filamentary magnetic current  $I_{m0}$  related to the electric current  $I_0$  flowing in a air-filled coil laying in the  $(x,y)$  plane by

$$I_{m0} \cong +j\omega\mu_0 I_0 NA / l \quad (1)$$

where  $N$  is the number of turns,  $A$  is the cross-sectional area and  $l$  is the overall length of the coil.

A multi-monostatic measurement configuration is considered: the case of bistatic configuration, with a fixed offset  $\Delta$  between the source and the receiver, can be easily taken into account by simple modifications of the formulas given below. The antenna system moves along the air-soil interface within the rectilinear observation domain  $\Sigma = [x = -x_M, x = x_M]$ . The objects are assumed to reside in the investigation domain  $D = [x = -a, x = a] \times [y = y_{min}, y = y_{min} + 2b]$ .

Our frequency domain formulation requires that measurements be performed at different frequencies in the operation bandwidth  $\Omega = [f_{min}, f_{max}]$ . The time convention  $\exp(+j\omega t)$  is assumed and omitted throughout the paper.

The unknown of the problem is the *contrast function*

$$\chi(x, y) = \varepsilon(x, y) - \varepsilon_s \quad (2)$$

that accounts for the difference between the equivalent dielectric permittivity of the target(s) and the background medium. The background equivalent dielectric permittivity  $\varepsilon_s$  is given by [9]

$$\varepsilon_s = \varepsilon_0 \varepsilon_r + \frac{\sigma_r}{j\omega} \quad (3)$$

where  $\varepsilon_r$  and  $\sigma_r$  are the relative dielectric permittivity and the electrical conductivity of the underground, respectively.

The datum of the problem is the scattered magnetic field  $H_s$ , defined as  $H_s = H_{tot} - H_{inc}$ , where  $H_{tot}$  is the total magnetic field accounting for the reflection from the air/underground interface and the backscattering from the targets, whereas  $H_{inc}$  is the incident magnetic field. We assume a simplified scattering model based on the Born Approximation (BA) [9, 24], implying that the total field in the investigation domain be equal to the incident field.

For the forward problem, i.e., the determination of the field scattered by a known target, the BA provides very accurate results under the assumption of weak scatterers, i.e., objects whose dielectric permittivity values are slightly different from the permittivity of the host medium and whose dimensions are small in term of probing wavelength [24]. This simplification leads to casting the imaging problem as the inversion of a linear operator [17, 18, 20]. In addition, the weak scatterer assumption can be relaxed by giving up “quantitative” reconstructions, while still achieving qualitative information about the targets in terms of detection, localization and rough estimation of their shape, as shown by a large number of numerical and experimental results [19, 20, 21].

Under the BA, a linear integral equation relating the magnetic scattered field to the contrast function is obtained as it follows. The magnetic field scattered by the targets can be expressed as the magnetic field radiated by the equivalent radiating sources

$$\mathbf{J}_{eq}(x, y) = j\omega[\varepsilon(x, y) - \varepsilon_s]\mathbf{E}_{inc}(x, y) = j\omega\chi(x, y)\mathbf{E}_{inc}(x, y) \quad (4)$$

where  $\mathbf{E}_{inc}$  represents the electric field radiated by the magnetic filamentary source within the investigation domain  $D$  in absence of the targets. The incident electric field is

$$\mathbf{E}_{inc} = E_{x,inc}\hat{x} + E_{y,inc}\hat{y} \quad (5)$$

due to the z-directed nature of the magnetic source. The equivalent radiating (electric) sources, using (4) and (5), are then rewritten as

$$\mathbf{J}_{eq} = j\omega\chi(x, y)(E_{x,inc}\hat{x} + E_{y,inc}\hat{y}) = J_{x,eq}\hat{x} + J_{y,eq}\hat{y}. \quad (6)$$

Therefore, the general formulation of the scattered magnetic field can be written as

$$\mathbf{H}_s(x, y) = j\omega \iint_D [G_{me,xz}(x, y, x', y')E_{x,inc}(x', y') + G_{me,yz}(x, y, x', y')E_{y,inc}(x', y')] \chi(x', y') dx' dy' \quad (x, y) \in \Sigma \quad (7)$$

where  $G_{me,xz}(x, y, x', y')$  and  $G_{me,yz}(x, y, x', y')$  account for the Green's function relating the z-component of the magnetic field (i.e., the only component of the magnetic field present in this problem) to the equivalent electric sources.

Finally, we cast the problem as the inversion of the linear integral equation (7) whose kernel is dictated by the incident

electric fields and Green's functions. These two quantities are dependent on the choice of the background scenario.

### III. HOMOGENEOUS BACKGROUND SCENARIO

In the case of antennas directly in contact with the interface air/soil, it is possible to assume, as a first approximation, a background scenario consisting of a homogeneous medium with the same electromagnetic properties of the underground. This assumption leads to analytical straightforward expressions for the incident field and Green's function. Starting from the magnetic field radiated by the filamentary magnetic current [26], the incident magnetic field is

$$H_{z,inc}(x', y') = \frac{-I_{m0}k_s^2}{4\omega\mu_0} H_0^{(2)}(k_s R) \quad (8)$$

where  $H_0^{(2)}(\cdot)$  is the Hankel function of second kind and zero-th order,  $k_s = \omega\sqrt{\epsilon_s\mu_0}$  is the underground wave number and  $R = \sqrt{(x'-x_s)^2 + y'^2}$  represents the distance between the source location  $(x_s, 0)$  and the sample point  $(x', y')$  in the investigation domain. From eq. (8), the incident electric field can be evaluated as

$$\mathbf{E}_{inc} = \frac{1}{j\omega\epsilon_s} \nabla' \times H_{z,inc} \hat{z} = \frac{1}{j\omega\epsilon_s} \left( \frac{\partial H_{z,inc}}{\partial y'} \hat{x} - \frac{\partial H_{z,inc}}{\partial x'} \hat{y} \right) \quad (9)$$

yielding

$$E_{x,inc} = \frac{1}{j\omega\epsilon_s} \frac{\partial H_{z,inc}}{\partial y'} = -j \frac{I_{m0}k_s y'}{4} \frac{H_1^{(2)}(k_s R)}{R} \quad (10)$$

Similarly,

$$E_{y,inc} = j \frac{I_{m0}k_s (x' - x_s)}{4} \frac{H_1^{(2)}(k_s R)}{R} \quad (11)$$

According to eq. (6), the equivalent current accounting for the target is

$$\mathbf{J}_{eq}(x', y') = \omega\chi(x', y') \frac{I_{m0}k_s}{4} H_1^{(2)}(k_s R) \left[ \frac{y'}{R} \hat{x} - \frac{(x' - x_s)}{R} \hat{y} \right] \quad (12)$$

Then, the magnetic field scattered by the equivalent electric source (12) is evaluated by separately considering two components of the equivalent electric current source given in (12). In particular, by exploiting vector potential theory [26], the  $x$ -component and  $y$ -components of the electric current can be expressed as

$$H_{z|J_x}(x_s, 0) = \iint_D G_{me,zx}(x_s, 0, x', y') J_x(x', y') dx' dy' = -\frac{jk_s}{4} \iint_D J_x(x', y') H_1^{(2)}(k_s R) \frac{y'}{R} dx' dy' \quad (13)$$

$$H_{z|J_y}(x_s, 0) = \iint_D G_{me,zy}(x_s, 0, x', y') J_y(x', y') dx' dy' = \frac{jk_s}{4} \iint_D J_y(x', y') H_1^{(2)}(k_s R) \frac{(x_s - x')}{R} dx' dy' \quad (14)$$

Finally, using (13) and (14), the general formulation of the scattered field is

$$H_z(x_s, 0) = \frac{jk_s}{4} \iint_D H_1^{(2)}(k_s R) \left[ \frac{(x_s - x')}{R} J_y(x', y') - \frac{y'}{R} J_x(x', y') \right] dx' dy' \quad (15)$$

Using (12) to rewrite the equivalent electric sources yields

$$\begin{aligned} H_z(x_s, 0) &= \frac{j\omega I_{m0} k_s^2}{16} \iint_D H_1^{(2)}(k_s R) \left[ -\frac{y'^2}{R^2} - \frac{(x_s - x')^2}{R^2} \right] \chi(x', y') dx' dy' \\ &= -\frac{jk_s^2 \omega I_{m0}}{16} \iint_D H_1^{(2)}(k_s R) \chi(x', y') dx' dy' \end{aligned} \quad (16)$$

The formulas above were obtained for single frequency and multi-monostatic configuration and with the antenna located at the interface ( $y=0$ ). Nevertheless, they are straightforwardly extended to the multi-frequency case, which is the case of interest for the inversion model.

#### IV. HALF-SPACE SCENARIO

In this improved formulation, the half-space scenario with a planar interface, see Fig. 1, is explicitly accounted for and spectral form formulas are obtained according to the guidelines given in [9, 17, 27, 28]. Similarly to the previous section, we begin with the magnetic field radiated at  $(x', y')$  in the underground by the impressed magnetic source  $I_{m0}$  located at  $(x_s, 0)$ . After simple manipulations, similar to the ones presented in [28], we obtain

$$H_{z,inc}(x', y') = -I_{m0} \frac{\omega \varepsilon_0}{2\pi} \int_{-\infty}^{+\infty} \frac{\varepsilon_s}{\varepsilon_s w_0 + \varepsilon_0 w_s} \exp[ju(x_s - x')] \exp[-jw_s y'] du \quad (x', y') \in D, \quad (17)$$

where  $w_0 = \sqrt{k_0^2 - u^2}$  and  $w_s = \sqrt{k_s^2 - u^2}$ , being  $k_0 = \omega \sqrt{\varepsilon_0 \mu_0}$  the wave number in the air. Then, the equivalent electric current, in the presence of the target, is evaluated as

$$\mathbf{J}_{eq}(x', y') = j\omega \chi(x', y') [E_{x,inc}(x', y') \hat{x} + E_{y,inc}(x', y') \hat{y}], \quad (18)$$

where

$$E_{x,inc}(x', y') = \frac{1}{j\omega\epsilon_s} \frac{\partial H_{z,inc}}{\partial y'} = \frac{I_{mo}}{2\pi} \int_{-\infty}^{+\infty} \frac{w_s \epsilon_0}{\epsilon_s w_0 + \epsilon_0 w_s} \exp[ju(x_s - x')] \exp[-jw_s y'] du \quad (19)$$

and

$$E_{y,inc}(x', y') = -\frac{1}{j\omega\epsilon_s} \frac{\partial H_{z,inc}}{\partial x'} = -\frac{I_{mo}}{2\pi} \int_{-\infty}^{+\infty} \frac{u \epsilon_0}{\epsilon_s w_0 + \epsilon_0 w_s} \exp[ju(x_s - x')] \exp[-jw_s y'] du \quad (20)$$

Finally, the scattered magnetic field at  $(x_s, y_s)$  is evaluated by exploiting the Green's function expressing the magnetic field in the upper medium radiated by an equivalent electric current located in the lower medium. In particular, for the filamentary current directed along the  $x$ -axis, the magnetic field directed along  $z$ -axis is

$$\begin{aligned} H_{slJ_x}(x_s, 0) &= \iint_D G_{me,zx}(x_s, y_s, x', y') J_{x,eq}(x', y') dx' dy' \\ &= \iint_D \underbrace{\int_{-\infty}^{+\infty} + \frac{1}{2\pi} \frac{w'_s \epsilon_0}{\epsilon_s w'_0 + \epsilon_0 w'_s} \exp[ju'(x_s - x')] \exp[-jw'_s y'] du'}_{\substack{\text{Equivalent Current} \\ \times \\ \text{x component of the incident E field}}} \times \\ &\quad \underbrace{\int_{-\infty}^{+\infty} \frac{1}{2\pi} \frac{w_s \epsilon_0}{\epsilon_s w_0 + \epsilon_0 w_s} \exp[ju(x_s - x')] \exp[-jw_s y'] du}_{\text{Electric Green's function from the transmitter to the target due to a magnetic current}} dx' dy' \\ &= \frac{j\omega\epsilon_0^2 I_{mo}}{4\pi^2} \iint_D \chi(x', y') \int_{-\infty}^{+\infty} \frac{w'_s}{\epsilon_s w'_0 + \epsilon_0 w'_s} \exp[ju'(x_s - x')] \exp[-jw'_s y'] du' \times \\ &\quad \int_{-\infty}^{+\infty} \frac{w_s}{\epsilon_s w_0 + \epsilon_0 w_s} \exp[ju(x_s - x')] \exp[-jw_s y'] du dx' dy' \end{aligned} \quad (21)$$

where  $w'_{0,s} = \sqrt{k_{0,s}^2 - u'^2}$ . For the electric filamentary source directed along the  $y$ -axis,

$$\begin{aligned}
H_{s|J_y}(x_s, 0) &= \iint_D G_{me,zy}(x_s, y_s, x', y') J_{y,eq}(x', y') dx' dy' \\
&\quad \underbrace{\text{Magnetic Green's function from the target to the receiver due to (equivalent) electric current}} \\
&= \iint_D \int_{-\infty}^{+\infty} \underbrace{-\frac{1}{2\pi} \frac{u' \varepsilon_0}{\varepsilon_s w'_0 + \varepsilon_0 w'_s}}_{\text{Equivalent current}} \exp[ju'(x_s - x')] \exp[-jw'_s y'] du' \times \\
&\quad \underbrace{\text{y component of the incident E field}} \\
&\quad \underbrace{\text{Electric Green's function from the transmitter to the target due to magnetic source}} \\
&= j\omega \chi(x', y') \times I_{m0} \int_{-\infty}^{+\infty} -\frac{1}{2\pi} \frac{u \varepsilon_0}{\varepsilon_s w'_0 + \varepsilon_0 w'_s} \exp[ju(x_s - x')] \exp[-jw_s y'] du dx' dy' \quad (22) \\
&= \frac{j\omega \varepsilon_0^2 I_{m0}}{4\pi^2} \iint_D \chi(x', y') \int_{-\infty}^{+\infty} \frac{u'}{\varepsilon_s w'_0 + \varepsilon_0 w'_s} \exp[ju'(x_s - x')] \exp[-jw'_s y'] du' \times \\
&\quad \int_{-\infty}^{+\infty} \frac{u}{\varepsilon_s w_0 + \varepsilon_0 w_s} \exp[ju(x_s - x')] \exp[-jw_s y'] du dx' dy'
\end{aligned}$$

Finally, by combining eqs. (21)-(22), we obtain

$$\begin{aligned}
H_s(x_s, 0) &= H_{s|J_x}(x_s, 0) + H_{s|J_y}(x_s, 0) \\
&= \frac{j\omega \varepsilon_0^2 I_{m0}}{4\pi^2} \iint_D \chi(x', y') \int_{-\infty}^{+\infty} \int_{-\infty}^{+\infty} \frac{w'_s w_s + u' u}{(\varepsilon_s w'_0 + \varepsilon_0 w'_s)(\varepsilon_s w_0 + \varepsilon_0 w_s)} \times \\
&\quad \exp[-j(w_s + w'_s) y'] \exp[j(u + u')(x_s - x')] du du' dx' dy' \quad (23)
\end{aligned}$$

Formula (23) may be easily extended to other measurement configurations exploiting observation diversity such as: single-view/multistatic one and multiview/multistatic configuration and to the case of an antenna system not close (in terms of probing wavelength) with the interface air/underground (see Appendix).

## V. TRUNCATED SINGULAR VALUE DECOMPOSITION AS INVERSION SCHEME

Under the Born approximation and for a two-dimensional and scalar geometry, the scattering phenomenon may be modelled through a linear scalar operator

$$A: \chi \in X \rightarrow H_s \in E \quad (24)$$

where  $\chi$  and  $H_s$  are the contrast function and the scattered magnetic field, respectively and  $X$  and  $E$  are assumed as Hilbert spaces of square integrable functions. In particular,  $X$  is the space of the unknowns and is made up of complex valued functions defined on the investigation domain  $D$ ;  $E$  is the data space and is made up of complex valued functions supported over  $\Lambda = \Sigma \times \Omega$  where  $\Sigma$  is the observation domain and  $\Omega$  the frequency band.

The choice of  $X$  and  $E$  as Hilbert spaces of square integrable functions accommodates the fact that no *a priori* information is available about the unknown, other than the finiteness of its "energy" as dictated by physical consideration. On the other end, it assures that  $E$  is "broad" enough to include the effect of uncertainties and noise on data. Thus, the determination of the contrast function amounts to inverting equation (24). The linear operators defined in eq. (16) and (23) are compact and accordingly the inverse problem at hand is an ill-posed problem [25].

For compact and non-symmetric operator (as the one at hand) the Singular Value Decomposition is a powerful tool to analyse and solve the problem. Accordingly, we denote by  $\{\sigma_n, u_n, v_n\}_{n=0}^{\infty}$  the singular system of the operator  $A$ ;  $\{\sigma_n\}_{n=0}^{\infty}$  is the sequence of the singular values ordered in a non-increasing way,  $\{u_n\}_{n=0}^{\infty}$  and  $\{v_n\}_{n=0}^{\infty}$  are orthonormal bases of the subspace that is the orthogonal complement of the kernel of  $A$  and of the closure of the range of  $A$ , respectively.

SVD provides a formal solution of the inversion of the functional equation, given by (24), as [25]

$$\chi = \sum_{n=0}^{\infty} \frac{\langle H_S, v_n \rangle_E}{\sigma_n} u_n \quad (25)$$

where  $\langle \cdot, \cdot \rangle_E$  denotes the scalar product in the data space  $E$ .

The lack of existence and stability of a solution can be remedied by regularizing the ill-posed inverse problem [29]. For its regularization, we exploit the *Numerical Filtering* or *Truncated Singular Value Decomposition* (TSVD), which is the simplest within the large class of windowing based regularization schemes [25]. Accordingly, the finite-dimensional approximate stable solution is

$$\tilde{\chi} = \sum_{n=0}^{N_T} \frac{\langle H_S, v_n \rangle_E}{\sigma_n} u_n \quad (26)$$

It is clear that, in addition to the computational convenience that dictates the choice of the regularization algorithm to be adopted, the key question is the choice of the regularization parameter  $N_T$ . This choice depends on the noise level, the mathematical features of the operator to be inverted and available *a priori* information about the unknown. Different methods exist to select the regularization parameter as the Morozov discrepancy principle or the generalized cross validation [30].

The regularization schemes, used to make stable the solution, impose constraints about the spatial variability of the unknown that is possible to be retrieved and equivalently about the resolution limits achieved by the linear inversion

model. The horizontal resolution improves as long as the extent of the measurement domain increases and/or the investigation point becomes closer and closer to the measurement domain [17, 28, 31]; in other words, the resolution limits improve when the investigated source point is viewed under a large angle by the measurement domain.

The in-depth resolution limits as long as the work frequency-band increases and/or the investigation point becomes closer and closer to the measurement domain. The effect of the extent of the measurement domain plays a secondary role compared to the frequency band [17, 19, 28, 31].

## VI. NUMERICAL RESULTS

Numerical analyses are presented for the two linear operators for the homogeneous and half-space background scenarios. The test cases considered refer to a non-magnetic soil with dielectric permittivity given by  $\epsilon_r = 10$  and conductivity  $\sigma_r = 0.001 \text{ S/m}$ . Referring to Fig.1, the targets are searched inside an investigation domain  $D$  of size  $20 \times 14 \text{ m}^2$ , which starts from the depth of 1 m, i.e.,  $a = 10\text{m}$ ,  $y_{\min} = 1\text{m}$ ,  $2b = 14\text{m}$ . The measurement line, at the air/soil interface, is centred on the investigation domain and is 15 m long; in this domain we locate 7 antennas spaced by a distance of 2.5 m. The operation frequency band for the inversion is  $\Omega = [5, 15] \text{ MHz}$ , with a frequency step of 1 MHz (11 discrete frequencies are exploited).

The reconstruction results refer to three different cases with a rectangular object simulating the section of a tunnel filled by air so that its dielectric permittivity is equal to the one of the free space. The tunnel has a cross section with extent equal to 3 m along  $x$ -axis and equal to 2m along the  $y$ -axis (depth).

The first three cases consider a tunnel centred with respect to the measurement domain and whose position (depth) is at a depth of 11 m (case 1); 8 m (case 2); and, 4 m (case 3). Scattered field data were generated with the Finite Difference Time Domain code GPRMAX [32], where the half-space scenario has been explicitly accounted for so that no approximations were made in their evaluation. Then, the scattered field data were Fourier transformed to the frequency domain where the inversion approaches work.

The first two subsections discuss the performance of the formulations for the target centred with respect to the measurement domain. The third subsection examines a comparison between the two formulations in the case of an offset target. The final subsection shows how a proper reformulation of the inverse problem mitigates the effects of faults in source elements by ensuring a reconstruction quality comparable to that achieved with the full dataset.

### VI. A) Homogeneous scenario

Using the results of Section III, we start by showing in Fig. 2 that the singular values behaviour has a smooth decay.

Here and in the following, we present the reconstruction results in terms of the normalized modulus of the contrast function with respect to its maximum in the investigation domain; in fact, the use of the BA makes it not feasible to achieve a quantitative reconstruction and thus the information that it is possible to retrieve is limited to the location and geometry of the target.

The first results refer to case 1 and Fig. 3 depicts the reconstruction for four different thresholds used as regularization parameter in the TSVD. In particular, TSVD thresholds refer to the number of terms  $N_T$  retained in TSVD expansion for the solution; for example, saying that the TSVD threshold is equal to -20 dB means that in the TSVD expansion (i.e., eq.(26)) only the terms corresponding to singular values larger than 0.1 times the maximum (first) singular value were retained.

The true position and geometry of the tunnel is depicted in these figures and the following ones by the rectangular box with black sides.

The reconstruction results point out that decreasing the TSVD threshold (i.e., increasing the number of terms retained in the TSVD) improves the reconstruction. For thresholds equal to -10 dB and -20 dB, the tomographic approach is not able to localize the tunnel; however, more accurate information about its position and the geometry is obtained with TSVD threshold equal to -30 and -40 dB, where reliable information is achieved for the transversal extent of the tunnel.

The second set of results refers to the case 2 and is depicted in figure 4. For this case, the reconstruction with TSVD at -20 dB already gives accurate information about the depth location of the tunnel also if the image appears blurred: the results improve for the TSVD threshold equal to -30 dB where a geometry estimation of the target is possible; the reconstruction with threshold equal to -40 dB is similar to the one of -30 dB.

Figure 5 depicts the results for case 3 with a shallower tunnel. In this case, the model error is higher due to the more significant mutual interactions between the target and the interface that are not accounted in the homogeneous medium model; this entails that more care has to be devoted to the choice of the TSVD threshold. For all the TSVD thresholds, the results appear worse compared to the other two cases especially for the geometry estimation and the case with threshold equal to -40 dB does not provide a reliable reconstruction.

### VI.B) Half-space formulation

Using the results of Section IV, Fig. 6 depicts the behaviour of the normalized singular values.

Case 1 results are given in Fig. 7; one notes that lower values of the TSVD threshold produce more accurate information for the localization and geometry of the tunnel. Compared to Fig. 3 (homogeneous scenario), the half-space formulation is able to achieve a good localization even with the TSVD threshold equal to -20 dB, which did not occur in the case of the homogeneous scenario.

Case 2 results are depicted in Fig. 8, and a comparison with Fig. 4 indicates that good agreement between the two formulations exists when the TSVD threshold is -30 dB.

Fig. 9 shows results for the shallower tunnel of Case 3. A comparison with Fig. 5 indicates that accounting for interface remarkably improves the localization and geometry estimation, especially for the cases of the TSVD threshold at -20 and -30 dB.

#### *VI.C) The case of an offset tunnel*

A tunnel centred at a depth of 8 m and at 4.5 m along the transverse direction is considered and Fig. 10 shows a comparison between the two formulations. The Green's function takes into account the refraction phenomenon within the half space. As a result, a better position localisation and tunnel geometry estimations are obtained, especially by comparing the results with TSVD threshold at -30 dB.

#### *VI.D) The case of the faults in the source arrays*

Finally, we deal with the effects of possible faults in some elements of the measurement array. As an example, we assume the case of two faults, i.e., the two antennas, located at 5 m and 7.5 m, are not working. This fault is simulated by setting to zero the corresponding data vector entry. For sake of brevity, we limit our exam to Case 2 (8 m tunnel depth) and for the homogeneous medium formulation.

Fig. 11 shows results obtained with the TSVD threshold equal to -30 dB when we assume the full measurement array but with the faults in the data; comparisons between Figs. 4.C and 11.A indicate that the reconstruction quality worsens compared to when no faults are present. Conversely, the reconstruction quality is improved when the inverse problem is reformulated by considering only the correctly operating sources, as shown in Fig. 11.B for the same TSVD threshold at -30 dB.

## **VII. CONCLUSIONS**

In this paper, the 2D problem of imaging underground structures using magnetic sources and receivers has been addressed. The data collection is performed in a classical multi-monostatic scenario, the most used in GPR applications for its simplicity, employing elementary loops as sources and by collecting the magnetic scattered field.

The inverse scattering problem is addressed by exploiting a linear inversion approach and by considering two different background scenarios: a homogeneous one (with the same properties of the underground) and a half-space geometry. The TSVD regularization scheme is used to obtain stable solutions of the inverse problem, where the regularization parameter is the number of terms of the TSVD expansion.

The performance of the two inversion strategies has been evaluated by performing qualitative reconstruction starting from the exact scattered field data, which are computed via a FDTD numerical code and then transformed to the Fourier domain. The result of the analyses is that the two strategies are comparable when the tunnel is underneath the synthetic aperture array; conversely in the case of shallower tunnel and of the offset tunnel the half-space model is superior because it accounts for electromagnetic effects due to the air-earth interface more accurately. Finally, we have presented a simple strategy able to account for faults in the transmitting or receiving elements based on a reformulation of the linear inverse problem by explicitly introducing knowledge of faulty elements.

Future research activities will be concerned with the extension of the proposed approaches to the improved multi-view/multi-static configuration [5-7] and the adoption of approaches able to account the inherent sparseness of the ground-penetrating radar scenario [33] with the aim to estimate the geometry of the target with more accuracy and resolution.

## **ACKNOWLEDGMENTS**

The authors are thankful to Dr. Jon A. Sjogren, US Air Force Office of Scientific Research, for sponsoring and funding this research under grant award number FA9550-05-1-0443.

## Appendix

The case of a mono-static antenna system located at distance  $y_s = -h$  (h distance along y of the antenna from the interface air-soil) is easily to be accounted for by assuming the propagation in free-space similarly to the strategy adopted in [34]; accordingly, the relevant scattered field integral becomes:

$$H_s(x_s, -h) = \frac{j\omega\epsilon_0^2 I_{mo}}{4\pi^2} \iint_D \chi(x', y') \int_{-\infty}^{+\infty} \int_{-\infty}^{+\infty} \frac{w'_s w_s + u'u}{(\epsilon_s w'_0 + \epsilon_0 w'_s)(\epsilon_s w_0 + \epsilon_0 w_s)} \times \exp[-j(w_s + w'_s)y'] \exp[-j(w_0 + w'_0)h] \exp[j(u + u')(x_s - x')] dudx'dy' \quad (27)$$

where the additional term  $\exp[-j(w_0 + w'_0)h]$  accounts for the propagation in air (from the transmitting and receiving side) from the interface to the antenna.

## References

- [1] P.T. Bellett and C.J. Leat, "Electrically small magnetic GPR antennas," *2003 IEEE Antennas and Propagation Society International Symposium*, vol.2, no., pp. 235- 238 vol.2, 22-27 June 2003.
- [2] T. J. Cui; A.A Aydiner, W. C. Chew; D.L. Wright, D.V Smith, "Three-dimensional imaging of buried objects in very lossy earth by inversion of VETEM data," *IEEE Trans. Geoscience and Remote Sensing*, vol.41, no.10, pp. 2197-2210, Oct. 2003
- [3] Le Gall, A.; Ciarletti, V.; Berthelie, J.-J.; Reineix, A.; Guiffaut, C.; Ney, R.; Dolon, F.; Bonaime, S. , "An Imaging HF GPR Using Stationary Antennas: Experimental Validation Over the Antarctic Ice Sheet," **Geoscience and Remote Sensing, IEEE Transactions on** , vol.46, no.12, pp.3975-3986, Dec. 2008.
- iform
- [4] M. Biancheri-Astier, V. Ciarletti, A. Reineix, C. Corbel, "Modeling the Configuration of HF Electrical Antennas for Deep Bistatic Subsurface Sounding," **IEEE Transactions on Geoscience and Remote Sensing**, vol.49, no.3, pp.1082-1091, March 2011
- [5] L. Lo Monte, D. Erricolo, F. Soldovieri, M.C. Wicks, "Radio Frequency Tomography for Tunnel Detection", **IEEE Transactions on Geoscience and Remote Sensing**, vol. 48, no.3, pp. 1128-1137, 2010
- [6] L. Lo Monte, D. Erricolo, F. Soldovieri, M.C. Wicks, " RF Tomography for below ground imaging of extended areas and close-in sensing", **IEEE Geoscience and Remote Sensing Letters**, vol. 7, pp. 496-500, 2010
- [7] M. C. Wicks, "RF tomography with application to ground penetrating radars," in *Proc. IEEE 41st ACSSC*, Nov. 4–7, 2007, pp. 2017–2022.
- [8] D. Colton, R. Kress, *Inverse acoustic and electromagnetic scattering theory*, Springer Verlag, 1992.

- [9] W. C. Chew, *Waves and Fields in Inhomogeneous Media*, IEEE Press, Piscataway, N.J., 1995.
- [10] R. Pierri, G. Leone, "Inverse scattering of dielectric cylinders by a second-order Born approximation," *Geoscience and Remote Sensing*, **IEEE Transactions on Geoscience and Remote Sensing**, vol.37, no.1, pp.374-382, Jan 1999
- [11] T. J. Cui, Y. Quin, Y. Ye, J. Wu, G. Wang, W. C. Chew, "Efficient Low-Frequency Inversion of 3-D Buried Objects With Large Contrasts," **IEEE Transactions on Geoscience and Remote Sensing**, Vol. GRS-44, No. 1, pp.3-9, Jan. 2006.
- [12] R. Persico, F. Soldovieri, "Two Dimensional Linear Inverse Scattering for Dielectric and Magnetic Anomalies" , **Near Surface Geophysics**, vol. 9, no. 3, doi: 10.3997/1873-0604.2010015, June 2011.
- [13] T. Isernia, V. Pascazio, and R. Pierri, "On the local minima in a tomographic imaging technique", **IEEE Transactions on Geoscience and Remote Sensing**, vol. 39, no. 7, pp. 1596-1607, Jul 2001.
- [14] G.A. Meles, J. Van der Kruk, S.A. Greenhalgh, J.R. Ernst, H. Maurer, A.G. Green, "A New Vector Waveform Inversion Algorithm for Simultaneous Updating of Conductivity and Permittivity Parameters From Combination Crosshole/Borehole-to-Surface GPR Data," **IEEE Transactions on Geoscience and Remote Sensing**, vol.48, no.9, pp.3391-3407, Sept. 2010
- [15] M. Pastorino "Stochastic Optimization Methods Applied to Microwave Imaging: A Review," **IEEE Transactions on Antennas and Propagation**, vol.55, no.3, pp.538-548, March 2007.
- [16] O. Lopera, E. C. Slob, N. Milisavljevic, S. Lambot, "Filtering Soil Surface and Antenna Effects From GPR Data to Enhance Landmine Detection," **IEEE Transactions on Geoscience and Remote Sensing**, vol.45, no.3, pp.707-717, March 2007.
- [17] G. Leone, F. Soldovieri, "Analysis of the distorted Born approximation for subsurface reconstruction: truncation

and uncertainties effect”, **IEEE Trans. Geoscience and Remote Sensing**, vol. 41, no. 1, pp. 66-74, Jan. 2003.

[18] T. J. Cui, and W. C. Chew, “Diffraction Tomographic Algorithm for the Detection of Three-Dimensional Objects Buried in a Lossy Half-Space,” **IEEE Trans. Antennas Propag.**, Vol. AP-50, No. 1, pp. 42-49, Jan. 2002.

[19] F. Soldovieri, A. Brancaccio, G. Prisco, G. Leone, R. Pierri, ”A Kirchhoff based shape reconstruction algorithm for the multimonostatic configuration: the realistic case of buried pipes”, **IEEE Transactions on Geoscience and Remote Sensing, IGARSS Special Issue**, Volume 46, no. 10, pp. 3031 – 3038, October 2008.

[20] F. Soldovieri, J. Hugenschmidt, R. Persico and G. Leone, “A linear inverse scattering algorithm for realistic GPR applications”, **Near Surface Geophysics**, vol. 5, no. 1, pp. 29-42, 2007.

[21] P. Meincke, “Linear GPR inversion for lossy soil and a planar air-soil interface”, **IEEE Trans. on Geoscience and Remote Sensing**, vol. 39, no.12, pp. 2713-2721, 2001

[22] R. Pierri, A. Liseno, R. Solimene, F. Soldovieri, “ Beyond physical optics SVD shape reconstruction of metallic cylinders”, **IEEE Trans. Anten. Propag.** Vol. 54, pp. 655-665, 2006.

[23] F. Soldovieri, R. Solimene, F. Ahmad, ” A fast data acquisition and processing scheme for through-the-wall radar imaging ”, *Proceedings of SPIE Conference 8021 Radar Sensor Technology XV*, June 2011, DOI: 10.1117/12.883746.

[24] M. Slaney, A. C. Kak, and L. E. Larsen, “Limitations of Imaging with First- Order Diffraction Tomography”, **IEEE Transactions on Microwave Theory and Techniques**, vol. MTT-32, no. 8, pp. 860-874, 1984. [17] M. Bertero and P. Boccacci, *Introduction to Inverse Problems in Imaging*. Bristol, U.K.: IOP, 1998.

[25] M. Bertero and P. Boccacci, *Introduction to Inverse Problems in Imaging*. Bristol, U.K.: IOP, 1998.

[26] C.A. Balanis, *Advanced Engineering Electromagnetics*. Wiley, 1989.

- [27] D. Lesselier, B. Duchene, "Wavefield inversion of objects in stratified environments: from back-propagation schemes to full solutions", in *Review of Radio Science 1993-1996*, pp. 235-268, ed. R. Stone, Oxford University Press, 1996.
- [28] R. Persico, R. Bernini, F. Soldovieri, "The role of the measurement configuration in inverse scattering from buried objects under the Born approximation", *IEEE Trans. Antennas and Prop.*, vol. 53, no. 6, pp. 1875-1887, June 2005.
- [29] C. De Mol, "A critical survey of regularized inversion methods" in *Inverse Problems in Scattering Imaging*, pp. 345-370, eds. M. Bertero and R. Pike, Adam Hilger, Bristol, 1992.
- [30] P.C. Hansen, J.G. Nagy. and D.P. O'Leary. *Deblurring Images: Matrices, Spectra and Filtering*, SIAM, Philadelphia, 2006.
- [31] F. Soldovieri, L. Crocco, "Electromagnetic Tomography", pp. 228-254 in *Subsurface Sensing*, (Editors Ahmet S. Turk, Koksal A. Hocaoglu, Alexey A. Vertiy ), Sep. 2011, Wiley Press, ISBN: 978-0-470-13388-0.
- [32] A. Giannopoulos, *GprMax2D V 1.5 (Electromagnetic Simulator for Ground Probing Radar)*, 2003.
- [33] Soldovieri, F.; Solimene, R.; Lo Monte, L.; Bavusi, M.; Loperte, A.; , "Sparse Reconstruction From GPR Data With Applications to Rebar Detection," **IEEE Trans. Instrumentation and Measurement**, vol.60, no.3, pp.1070-1079, March 2011.
- [34] R. Persico, " On the role of measurement configuration in contactless GPR data processing by means of linear inverse scattering", **IEEE Trans. Antennas and Prop.**, vol. 54, no. 7, pp. 2062-2071, July 2006.

## Figures

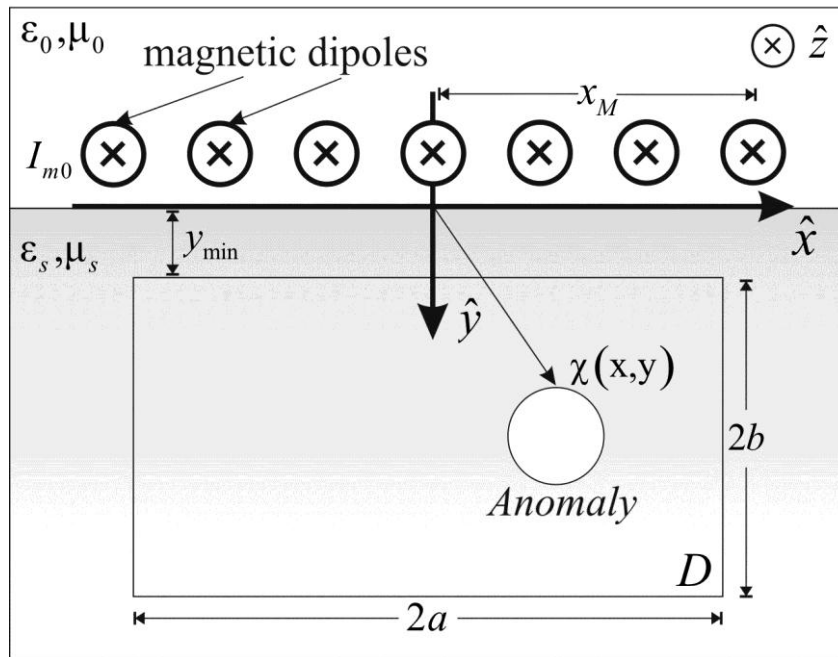


Figure 1. Geometry of the problem

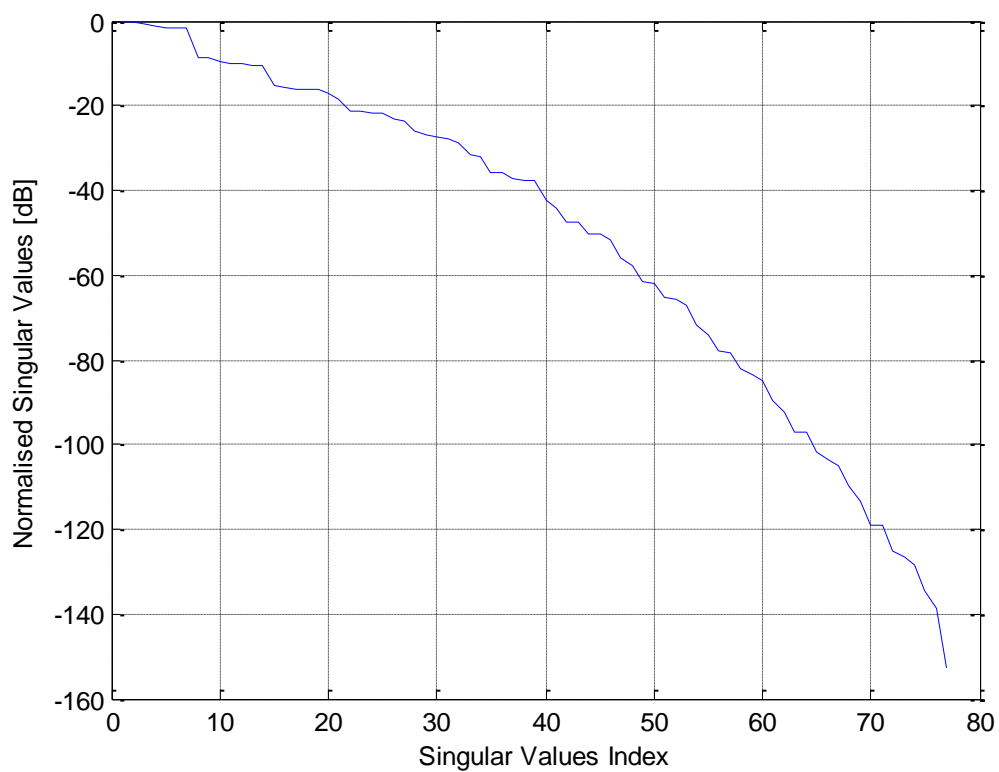
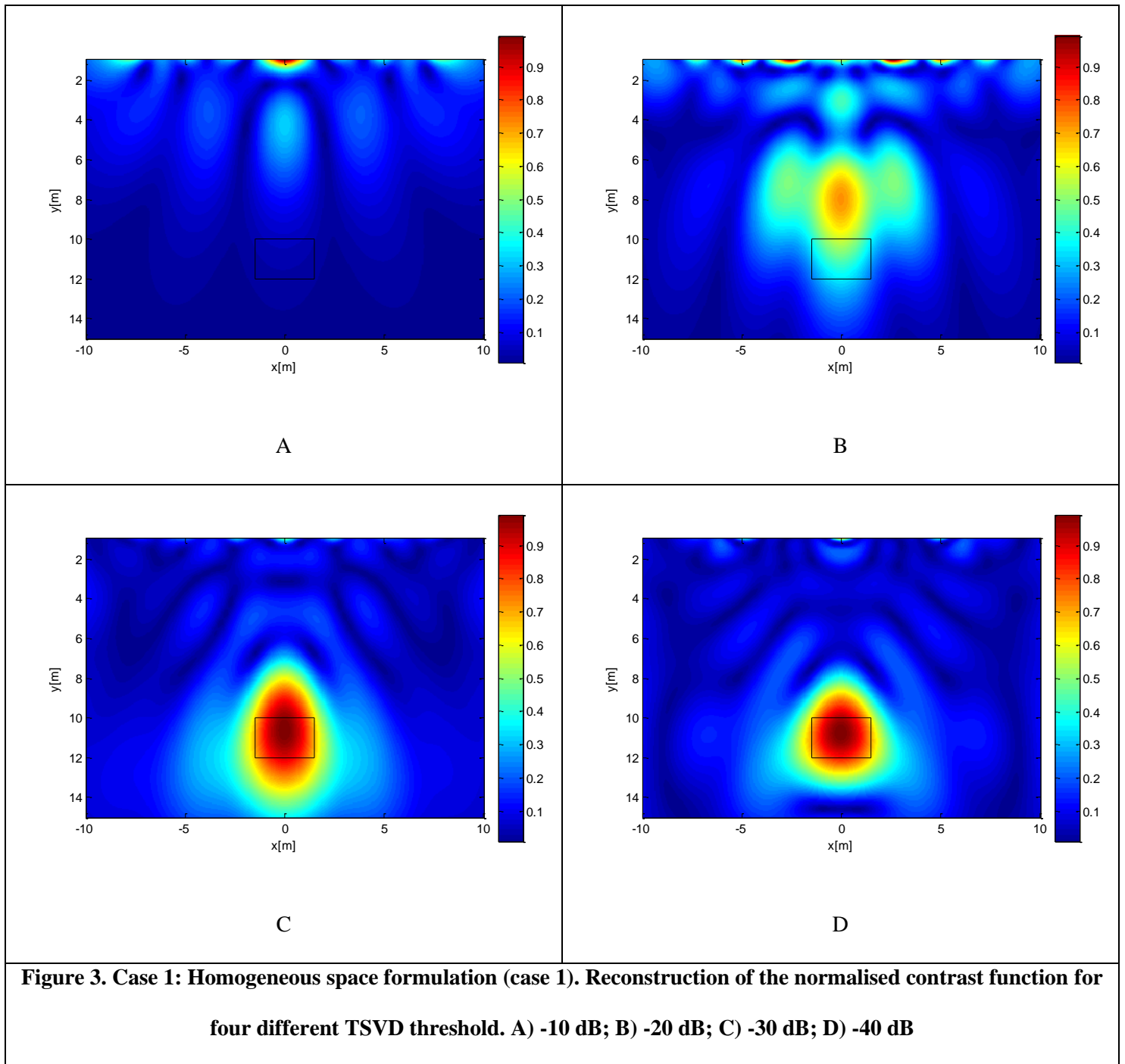
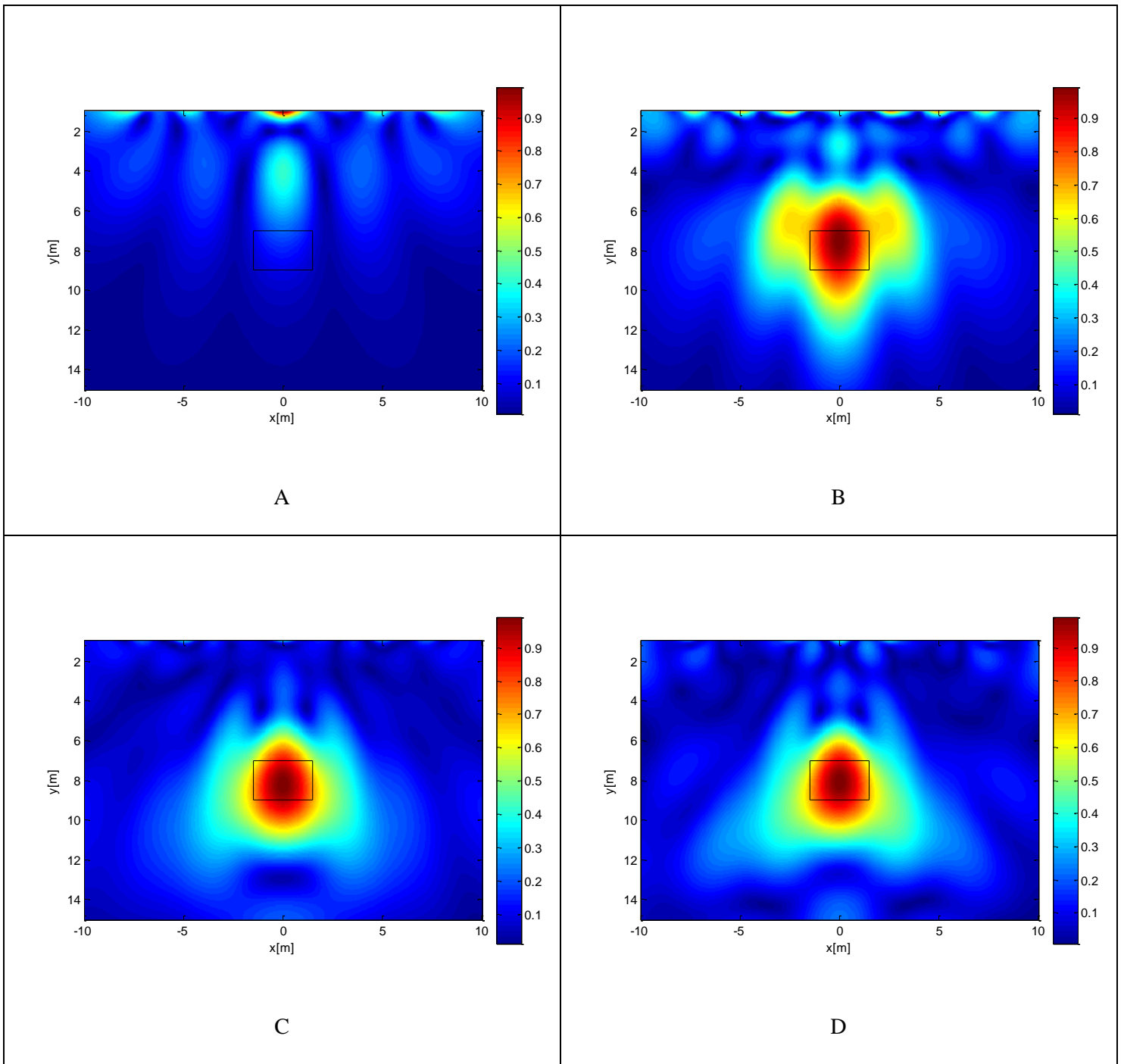
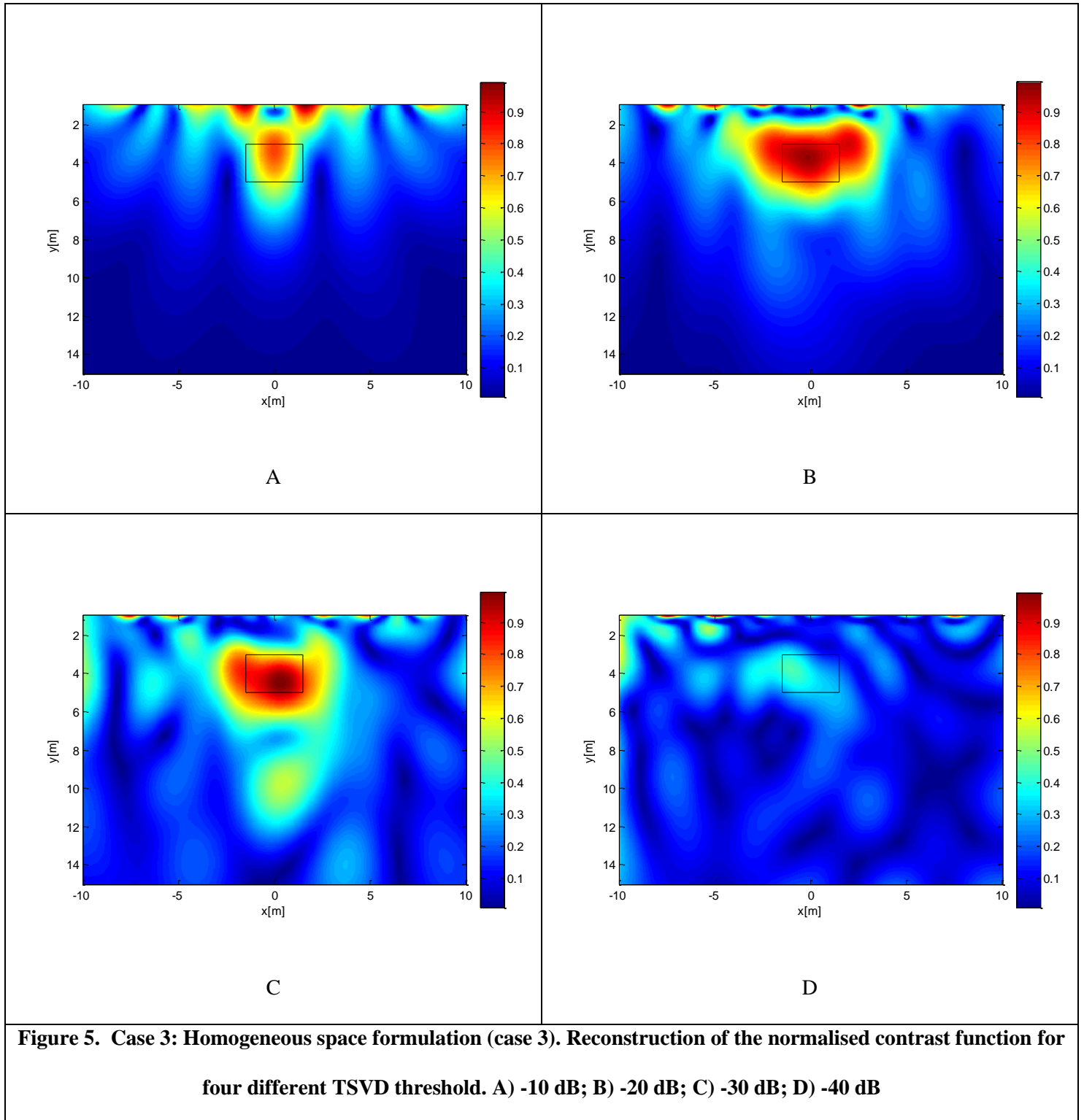


Figure 2. Normalised Singular Values for the case of the homogeneous background scenario

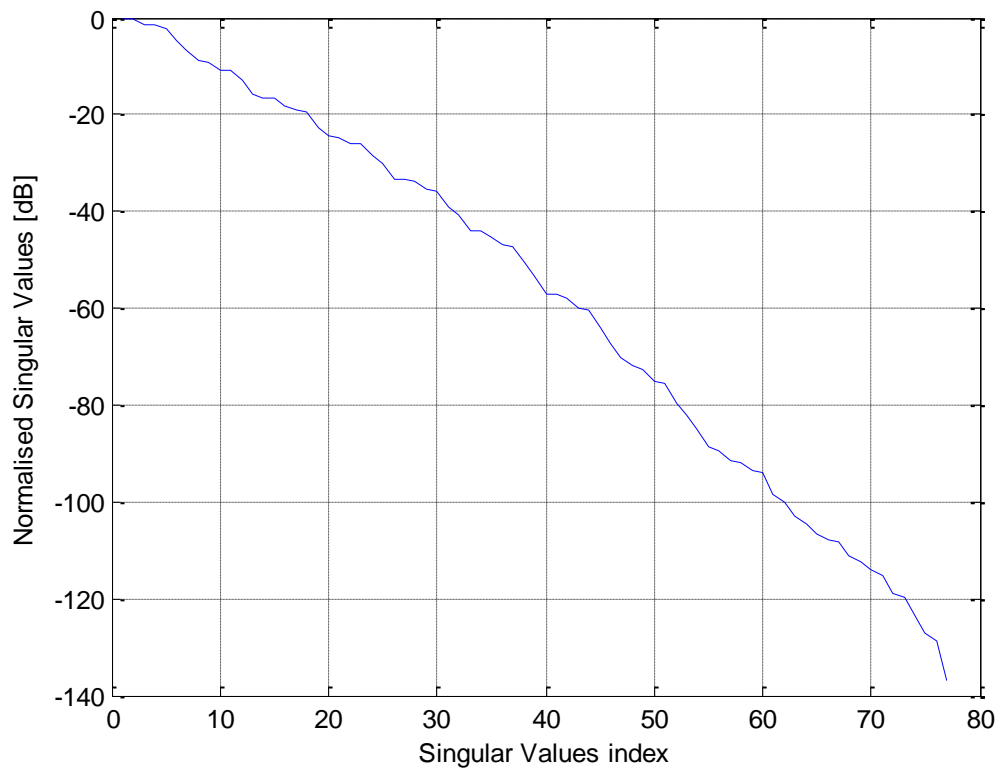




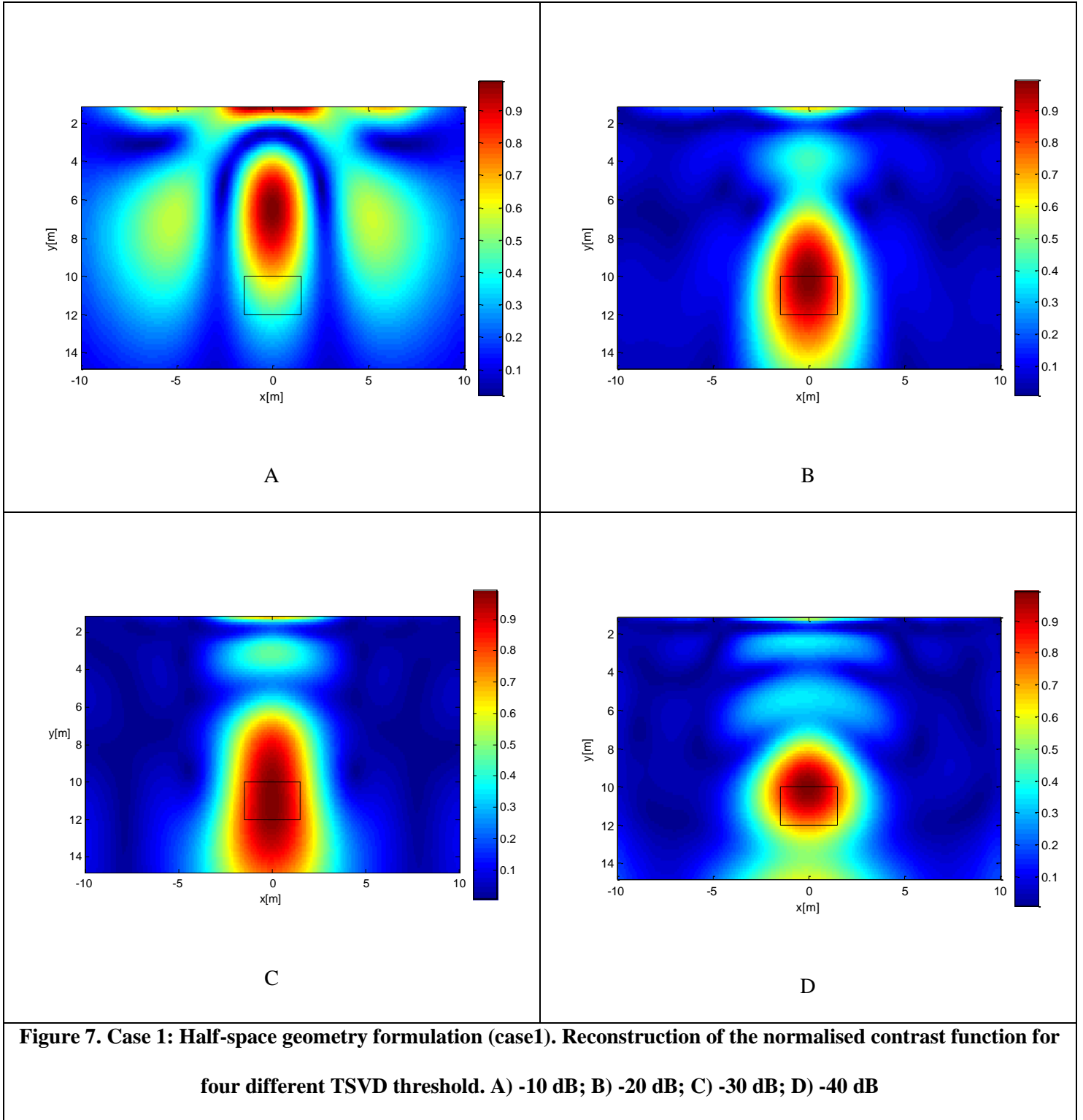
**Figure 4. Case 2: Homogeneous space formulation (case 2). Reconstruction of the normalised contrast function for four different TSVD threshold. A) -10 dB; B) -20 dB; C) -30 dB; D) -40 dB**

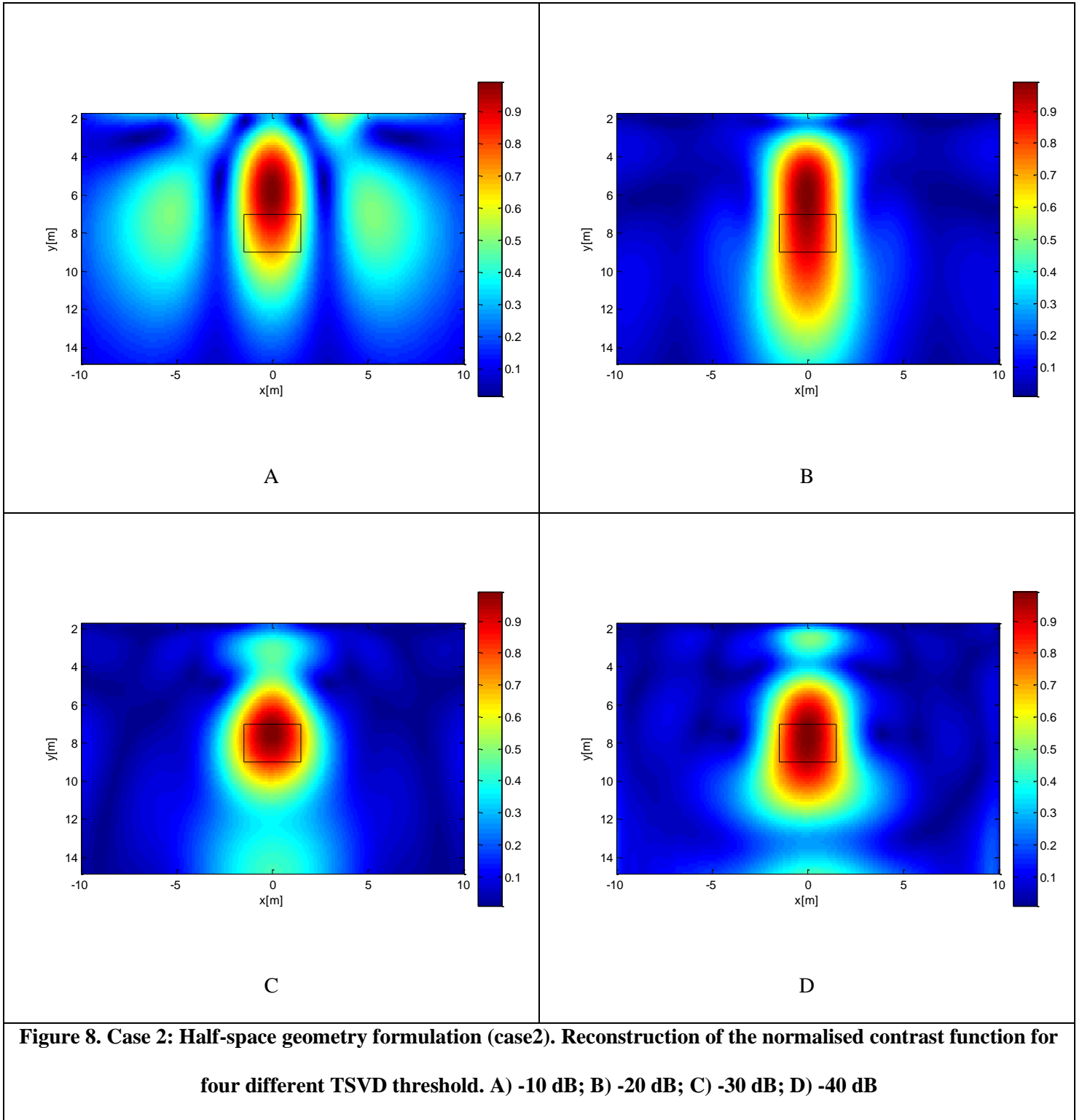






**Figure 6. Normalised Singular Values for the case of the half-space background scenario**





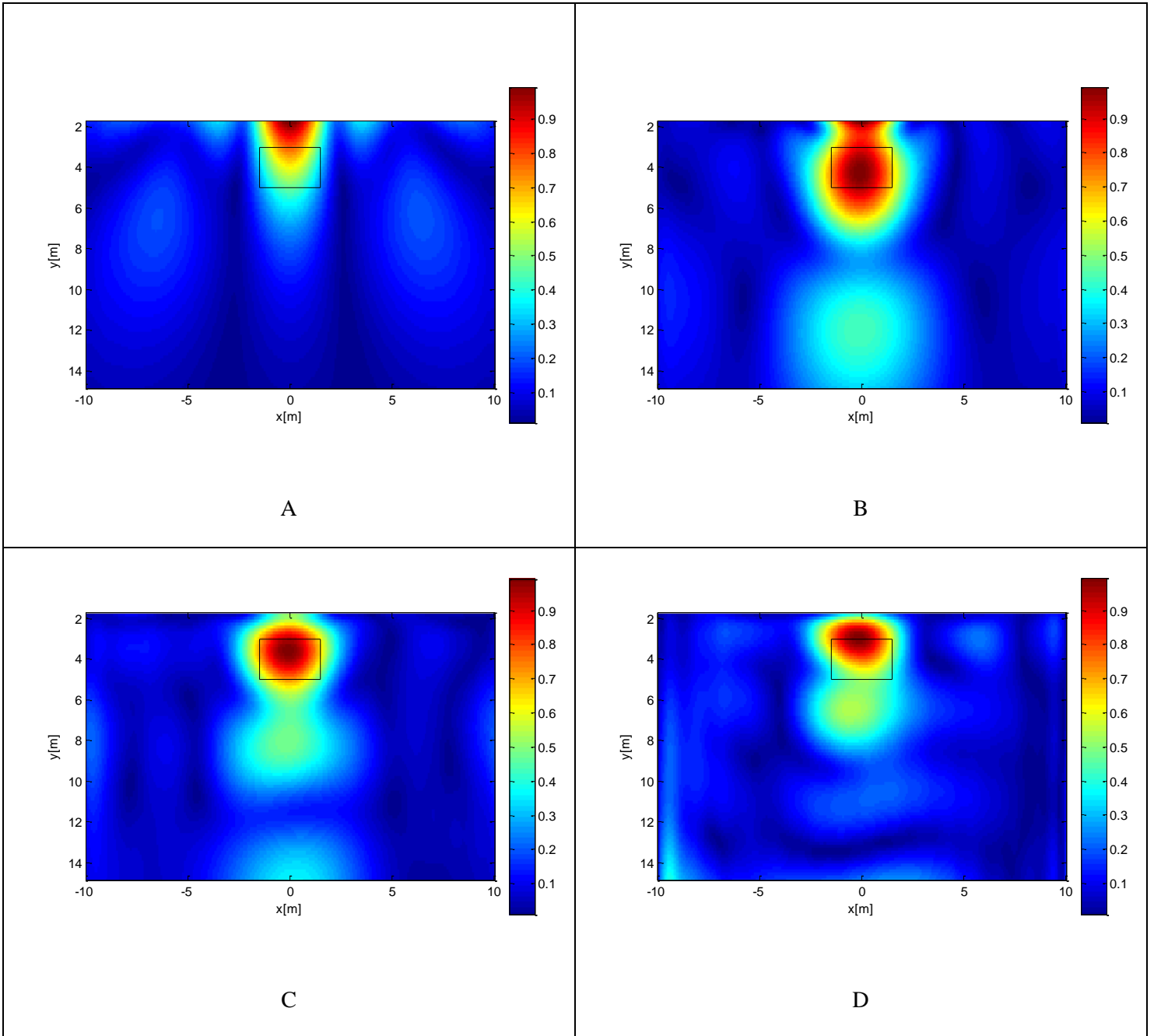


**Figure 9. Case 3: Half-space geometry formulation (case 3). Reconstruction of the normalised contrast function for four different TSVD threshold. A) -10 dB; B) -20 dB; C) -30 dB; D) -40 dB**

